Int. J. Heat Mass Transfer. Vol. 33, No. 6, pp. 1299–1306, 1990
Printed in Great Britain

0017-9310/90 $3.00 + 0.00

Mass transfer of supersaturated contaminants in cryogenic helium heat exchangers

HO-MYUNG CHANG and JOSEPH L. SMITH, JR.
Department of Mechanical Engineering, MIT Room 41-208, Massachusetts Institute of Technology, Cambridge, MA 02139, U.S.A.

(*Received 5 July 1988 and in final form 5 September 1989*)

Abstract—A new experimental technique is developed to measure the distribution of frost accumulated inside the passage of a cryogenic helium heat exchanger. The frost is accumulated by condensation of a contaminant on the passage wall during steady-flow operation of the balanced counterflow heat exchanger. The distribution is measured by flushing the accumulated contaminant into a detector at the exit of the passage. A heat source is moved from the cold to the warm end to convert the spatial distribution of the contaminant to concentration as a function of time in the exiting helium stream. When the degree of supersaturation is small, the accumulation distribution agrees reasonably well with the analytical solution without snow formation. As the supersaturation increases, a clear secondary peak in the distribution is observed, which results from the formation of snow in the free stream and its subsequent deposition as frost on the wall. Based on the results, an onset condition is developed for the formation of snow of a supersaturated contaminant in helium.

1. INTRODUCTION

FROST formation of contaminants in helium is frequently encountered in cold heat exchange apparatus. A typical example is the freeze-out process used for helium purification [1, 2]. Most impurity gas is removed from the stream by solidification as a frost on the cold wall when the mixture is cooled below the frost temperature. A similar process occurs in the operation of a cryogenic refrigeration or liquefaction system the working fluid of which has a certain level of impurity. Accumulated solid contaminants inside the system reduce the efficiency and results in scheduled or unscheduled stoppage after a period of operation. Another example of frost formation of minor gases in helium is the trapping of components separated by a gas chromatography column [3]. The helium carrying the separated components is introduced into a cold heat exchanger to freeze-out the component for further analysis.

This experimental study investigates the mass transfer characteristics of a contaminant in helium flowing inside a round tube, which is one passage of a balanced counterflow heat exchanger with a constant axial temperature gradient. When helium containing a very small fraction (of the order of 100 ppm or less) of a contaminant, flows in the direction of decreasing temperature, it reaches the frost temperature of the contaminant at the point where the partial pressure of the contaminant equals its saturation pressure. From this point ($x = 0$), the contaminant starts to frost as solid on the wall as shown in Fig. 1(a), since the wall temperature is lower than the gas temperature as shown in Fig. 1(b). The local concentration is radially uniform at the frost starting point. As the contaminant is accumulated on the wall as frost, the concentration of contaminant near the wall is smaller than that near the center of the tube, which results in a net mass transfer of contaminant to the wall by molecular diffusion. The amount of mass transfer to the wall increases along the axis at the beginning, but decreases as the concentration profile gets fully

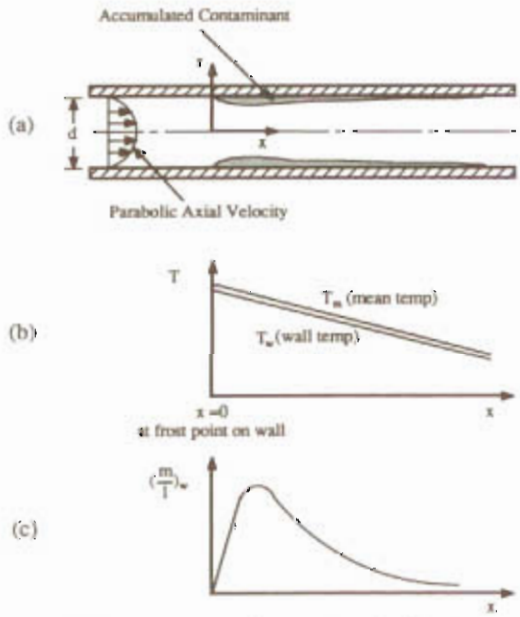

FIG. 1. Wall accumulation of contaminant in fully developed laminar flow through a round tube: (a) schematic of wall accumulation ($x = 0$ at frost point); (b) linear axial temperature distribution; (c) typical distribution of wall accumulation per unit length without snow.

NOMENCLATURE

A	cross-sectional area of tube, πr_0^2
a_n	nth coefficient in series solution
c	concentration of contaminant [kg m^{-3}]
c_p	specific heat at constant pressure
c_s	saturation concentration of contaminant
c_0	inlet concentration of contaminant
D	mass diffusivity of contaminant in helium [m^2 s^{-1}]
d	tube diameter
DSS	degree of supersaturation, defined by equation (7) [dimensionless]
h_{ig}	latent heat of sublimation
L_{det}	detector length in Fig. 4
L_{test}	test length in Fig. 4
Le	Lewis number, α/D
$\dot{m}$	mass transfer rate [kg s^{-1}]
p	partial pressure of contaminant
p_s	saturation pressure of contaminant
p_{tot}	total pressure of mixture
$\dot{q}$	heat transfer rate [kW]
R	gas constant of contaminant [kJ kg^{-1} K^{-1}]
R_n	nth eigenfunction of the Graetz solution
r	radial coordinate
r_0	tube radius
Re	Reynolds number, $u_m d/\nu$
Sc	Schmidt number, ν/D
T	temperature
t	time
u_m	axial mean velocity
v_h	heater speed
x	axial coordinate, $x = 0$ at frost point.

Greek symbols

α	thermal diffusivity
η	dummy variable
λ_n	nth eigenvalue of the Graetz equation
ν	kinematic viscosity
ξ	dummy variable
σ	snow deposition width.

Subscript

w	tube wall.

developed because the saturated concentration decreases slowly as temperature decreases. A typical axial distribution of wall accumulation is shown in Fig. 1(c).

The above description is true when the contaminant condenses only at the tube wall. Since the Lewis number (α/D) of every common contaminant in helium is greater than unity (2.5–3.0 at standard conditions), the heat transfer through helium is relatively faster than the mass transfer of the contaminant to the wall for laminar flow conditions. Thus, for some region near the wall, the local partial pressure of the contaminant is greater than the saturation pressure corresponding to the local temperature as sketched in Fig. 2 so that supersaturation of the contaminant always occurs. This implies a possibility of nucleation

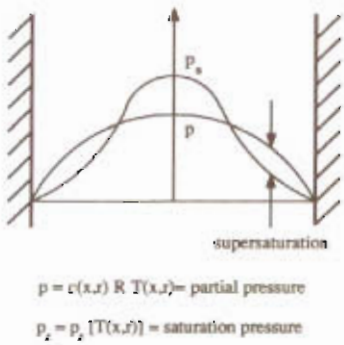

FIG. 2. Sketch for relative profile of contaminant partial pressure to its saturation pressure in fully developed supersaturated flow.

to form snow at a distance from the wall. Of special interest in this study is an experimental verification of the onset of snow formation in the laminar free stream. To simplify the analysis of the supersaturated mass transfer, it is assumed that the mass transfer of the contaminant is uncoupled from the momentum and heat transfer of helium. This is valid when the mole fraction of the contaminant is very low and the thickness of wall accumulation is small compared with the tube diameter.

The possibility of the formation of solid particles in a laminar free stream due to supersaturation was discussed earlier by Bailey [2] in a paper on the freeze-out purification of a gas. Snow formation criteria were qualitatively treated for the flow of an air–water–vapor mixture by Chen [4]. As far as the authors are aware, the formation of snow from a supersaturated minor gas has not been clearly verified previously. One of the reasons is that supersaturation is not so significant in the cooling of humid air flow below its frost temperature (for example, refs. [4–6]). Another reason is that the typical experimental methods of visual observation for solid formation [5, 7, 8] are not suitable for the conditions of this investigation. A recent analytical study by the authors gave an exact solution for the distribution of wall accumulation in the case of no snow formation, and showed that the onset of snow could be predicted by the degree of supersaturation [9].

A crucial quantity in the problem is the spatial distribution of contaminant accumulation on the tube wall. The basic idea of the method to detect the dis-

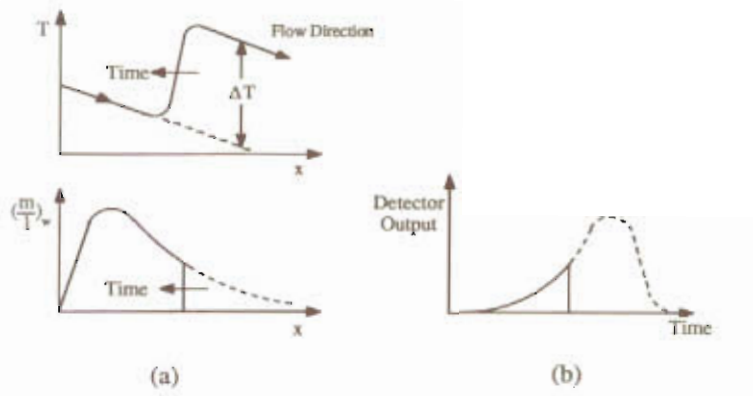

FIG. 3. Schematic of experimental detection technique for spatial distribution of wall accumulation: (a) propagation of sharp temperature wave from the cold end; (b) monitoring of concentration with detector.

tribution is shown in Fig. 3. After the test column is contaminated in well-posed conditions, a sharp temperature wave generated by a continuously moving heat source is propagated from the cold to the warm end (opposite to the flow direction), flushing the accumulated contaminant as shown in Fig. 3(a). A detector measures the concentration of the contaminant in the helium stream at the exit of the column. The time history of the detector output (Fig. 3(b)) reflects the spatial distribution, if the continuous heating is locally very intensive and the dispersion of the concentration is minimized. Since an analytical solution for the accumulation distribution without snow formation is available [9], the experimental results are compared with the analytical solution to obtain a fundamental understanding for the behavior of supersaturated contaminant.

2. EXPERIMENT

2.1. *Apparatus*

A simplified schematic of the experimental system is shown in Fig. 4 (for complete details, see ref. [11]). The test column is the center tube of a concentric tube counterflow heat exchanger. The outer cold to warm stream is not shown in [illegible] placed vertically [illegible] chamber for [illegible] insulation. The warm (top) end of the test column is at room temperature and the cold (bottom) end is maintained at around 110 K by liquid propane. The column is a stainless steel capillary tubing of 1.0 mm i.d. and 2 m long. The test gas with a concentration of 100 ppm of CO_2 (calibration gas, Matheson Gas Products, Newark, New Jersey) is fed into the column from the top.

An outer tube having 9.5 mm o.d. and 0.7 mm wall thickness is placed around the concentric tube heat exchanger and is filled with liquid propane to control the column temperature distribution. Propane is used because at moderate pressure it remains in the liquid phase from room temperature to liquid nitrogen temperature. The liquid phase is essential to the temperature control as described later. The propane is cooled by a liquid nitrogen bath. The tubes, the nitrogen bath, and the vacuum chamber are stainless steel.

A wire heater is uniformly wrapped along the outer tube containing the propane to produce an axially uniform heat flux (not explicitly shown in Fig. 4) which establishes the linear temperature distribution prior to the start of contaminant accumulation. In order to generate a sharp temperature wave, as shown in Fig. 3(a), another small heater is located between the test column and the outer tube and is movable in the axial direction. The axial position is precisely controlled by a lead wire and a d.c. stepper motor (Airpax Co. model K82227) at the top of the apparatus. The moving heater is a thermofoil heater ($R = 26.1\ \Omega$) with Kapton insulation (Minco Product, Minneapolis, Minnesota) and is attached by epoxy to a short piece of relatively thick tube.

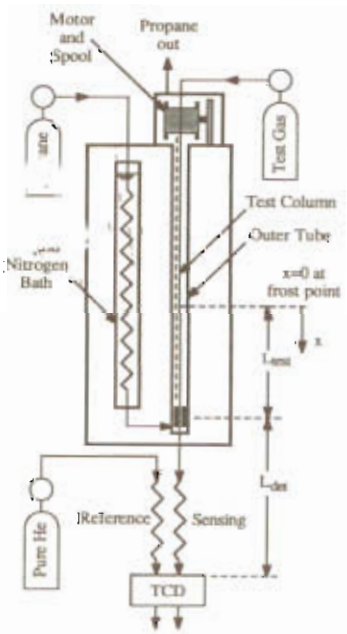

FIG. 4. Simplified schematic of experimental apparatus.

The detector is a fast response thermal conductivity detector (TCD) installed in a gas analyzer unit (Gow-Mac Instrument Co., Bound Brook, New Jersey, Model 50-450), which is used typically for gas chromatography (GC) applications. The cells of the TCD have been designed to be very small to avoid too much dispersion in the detector output. The response time is less than 1 s.

2.2. *Instrumentation*

The pressures and the flow rates of test gas and reference gas are controlled by two identical two-stage pressure regulators and flowmeters. Temperatures at two TCD inlets are maintained the same with a parallel-flow heat exchanger.

The temperature control of the test column is the most important part of the experiment. Two control actions are required. The first in time sequence is to set a linear temperature gradient before any helium flow through the column. This requirement is achieved by combining a cold liquid propane flow through the outer tube and an axially uniform heat flux on it. If the small temperature dependence of c_p is neglected for liquid propane, the linear temperature gradient is obtained as

$$-\frac{\partial T}{\partial x} = \frac{(\dot{q}/l)}{(\dot{m}c_p)_{prop}} \tag{1}$$

where the numerator of the right-hand side is the uniform heat flux per unit axial length. The flow of test gas in the test column does not affect the temperature distribution, because the heat capacity of the helium is negligible relative to that of liquid propane.

The second control action is to generate a sharp temperature wave as shown in Fig. 3(a). An optimum wave speed is determined by two factors. A slower speed results in more detailed information for the spatial distribution. Too slow speed, however, cannot generate the required steep temperature front because more time is allowed for axial thermal diffusion. An acceptable speed has been selected as 1 cm s^{-1} from a numerical simulation. The temperature increase of the tubes and liquid propane (ΔT in Fig. 3(a)) should be about 50 K to guarantee that all of the accumulated contaminant will evaporate into the helium stream. The heat flux to produce the temperature wave is 1.0×10^5 W m^{-2}. Burnout of the thermofoil heater is avoided with subcooled boiling of liquid propane. The bubbles are expected to condense immediately because the cold wall is very close to the heating surface.

Temperature of the column is measured by thermocouple soft-soldered on the outer tube at six locations—one at the cold end, three 10 cm apart above the cold end, and two 60 cm apart. The temperature difference between the thermocouple location and the test column at the same axial position is negligible while the linear temperature is maintained during the steady flow accumulation. When the intensive local heating is applied, the thermocouple temperature increases earlier than the column temperature. This is taken into account when detector output is related to wall accumulation distribution.

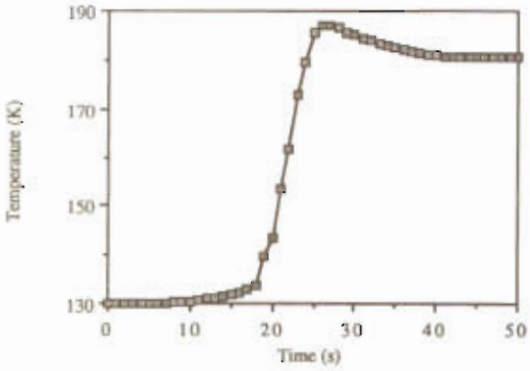

FIG. 5. Time history of temperature at 20 cm above the cold end during detection phase.

The detector output is recorded in units of ppm of CO_2. The data are collected every second through an ACRO Data Acquisition and Control System. The sampling time, 1 s, can be interpreted as a sampling length of 1 cm on the wall accumulation of the test column, because the temperature wave moves at the speed of 1 cm s^{-1}.

2.3. *Procedure*

The experiment consists of three phases—the linear temperature set-up, the contaminant accumulation, and the detection. After the vacuum chamber and the gas analyzer are ready, the test column temperature is set linear by a constant propane flow through the outer tube and a uniform heat flux over the tube according to equation (1). The pressure of propane in the tube is kept at 460 kPa by a back pressure regulator at the exit of the tube, where the boiling temperature of propane is 273 K. Near the top plate, most of the propane is vaporized and the stepper motor is operated in a vapor-filled enclosure.

When the desired temperature distribution is obtained, the flow of test gas is started through the test column. To insure the steady state of the temperature, the propane flow and the heat flux are maintained at the same conditions as during the temperature set-up phase. The accumulation time is 4–5 min.

To start the detection, the propane flow and the heat flux are shut off at the same time. Immediately after that, the moving thermofoil heater (placed at the cold end before moving) and the stepper motor are turned on to propagate the temperature wave from the cold end. During this period, the TCD detects and records the concentration of contaminant in the helium leaving the column. In order to avoid subsequent accumulation of the contaminant, the temperature of the column downstream of the heater is raised to a level above the saturation temperature of the peak concentration.

The time history of temperature at a point 20 cm above the cold end is shown in Fig. 5. The time axis

is zero when the moving heater starts to move. The temperature is increased by 50 K within 7 s after the top of the heater reached the point at $t = 18$ s. The small amount of preheating is due to the natural convection in the liquid propane. The overshoot at the end of heating is mainly due to the condensation of tailing bubbles. Since most of the contaminant accumulation at a given location sublimates back to vapor at 140–150 K (within 2 s), the heating rate is considered satisfactory.

3. RESULTS AND DISCUSSION

3.1. *Experimental results*

Tests were run with the 100 ppm of CO_2 in He at various flow rates and total pressures. Only three critical results are presented and discussed due to space limitations (for details, see ref. [11]). The three tests were performed at the same total pressure and almost the same axial temperature gradient, but at three different flow rates. Concentrations of CO_2 as a function of time from the detector are shown in Fig. 6. Since the evaporated contaminant is carried at the test flow rate, the response appears earlier as the flow rate increases. The 100 ppm concentration at the end of the response is the inlet value because the temperature of the column after heating is everywhere higher than the frost point of the test gas.

To convert the time history of the TCD output to the spatial distribution of wall accumulation in the test column, it would be necessary to formulate and solve an integral equation for the dispersion mechanism. Instead of the unnecessarily lengthy and complicated procedure, a simple coordinate transformation for ideal detection is done here assuming a point heater, no diffusion, and an instant response of the TCD. The amount of dispersion is considered when the experimental and analytical distributions are compared. Thus the mass accumulation per unit axial length of tube wall can be related to the concentration at the TCD by

$$\left(\frac{m}{l}\right)_s = \frac{Ap_{tot}}{RT}\left(1+\frac{u_m}{v_h}\right)(10^{-6})(\text{ppm of } CO_2) \quad (2)$$

where the total pressure, p_{tot}, and the temperature, T, are the values at the detector, u_m the mean velocity of the test gas and v_h the heater speed in the negative x-direction. With the notations in Fig. 4, the axial location of accumulation is related to the time at the TCD by

$$x = L_{tot} - \left(t - \frac{L_{det}}{u_m}\right)v_h. \quad (3)$$

3.2. *Analytical solution without snow*

An analytical solution for the accumulation distribution was obtained [9] on the assumption that no snow was formed in spite of supersaturation. In the solution, the mass transfer of contaminant was

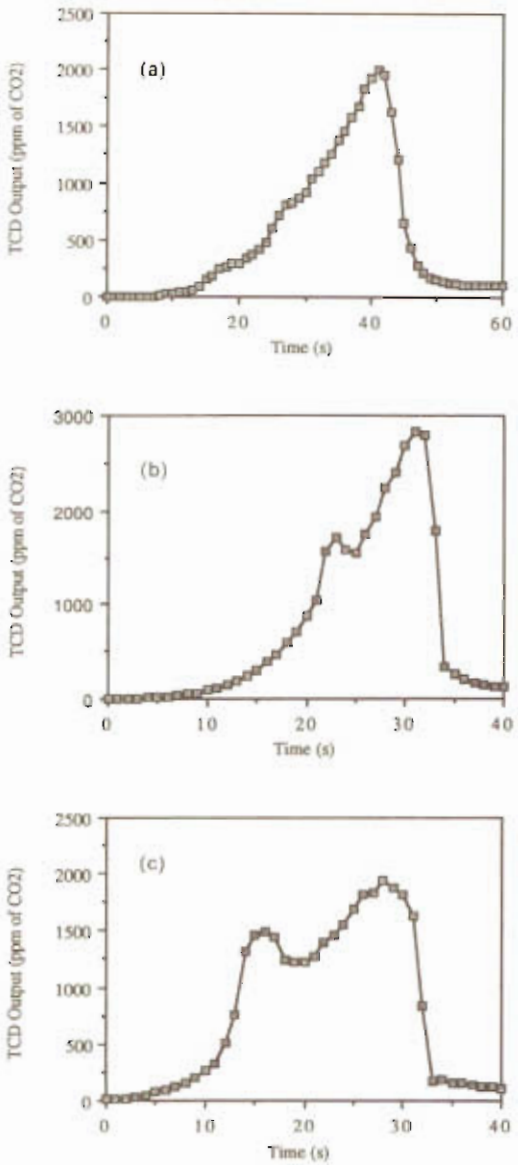

FIG. 6. TCD outputs of three runs ($p_{tot} = 191$ kPa): (a) Run 1 ($Re = 11.5$, $dT/dx = -70.2$ K m^{-1}); (b) Run 2 ($Re = 19.1$, $dT/dx = -74.3$ K m^{-1}); (c) Run 3 ($Re = 26.7$, $dT/dx = -66.5$ K m^{-1}).

assumed to be uncoupled from the momentum and the heat transfer, because the phase change and accumulation of the low-concentration contaminant did not affect the temperature distribution. For steady laminar conditions, the axial convection of the contaminant is balanced by molecular diffusion in the radial direction. Thus

$$2\left[1-\left(\frac{r}{r_0}\right)^2\right]\frac{\partial}{\partial x}[u_m(x)c] = \frac{D(x)}{r}\frac{\partial}{\partial r}\left(r\frac{\partial c}{\partial r}\right). \quad (4)$$

The boundary conditions are given by

$$c(x=0,r)=c_0$$

$$\frac{\partial c}{\partial r}(x,r=0)=0,\quad c(x,r=r_0)=c_s(x)\quad \text{for}\quad x\geqslant 0 \tag{5}$$

because the local concentration of contaminant is radially uniform at the frost point ($x = 0$) and is the saturation concentration at the surface of the frost on the wall ($r = r_0$). The equation for $c(x, r)$ is solved by the same method as used for a heat transfer problem with an arbitrary wall temperature [10]. The solution for the mass accumulation rate per unit axial length has been shown [11] to be

$$\left(\frac{\dot{m}}{l}\right)_w = 2\pi D(x)\sum_{n=0}^{\infty} a_n R_n'(1)\int_{\xi=0}^{x}\frac{u_m(\xi)}{u_m(x)}\times\exp\left(-\int_{\eta=\xi}^{x}\frac{\lambda_n^2}{Re\,Sc}\frac{\mathrm{d}\eta}{r_0}\right)\frac{\mathrm{d}c_s}{\mathrm{d}\xi}\,\mathrm{d}\xi \tag{6}$$

where λ_n and R_n are the nth eigenvalue and eigenfunction of the so-called Graetz equation, respectively, and a_n is the nth coefficient of the series expansion of a function $f(r) = 1$ in terms of $R_n(r)$. The binary mass diffusivity, D, the mean axial velocity, u_m, and the saturation concentration, c_s, are x-dependent and determined by the axial temperature distribution.

3.3. *Onset of snow*

The coordinate-transformed accumulations derived from the TCD outputs with equations (2) and (3) are shown in Fig. 7 along with corresponding analytical results without snow, which is the mass accumulation rate of equation (6) multiplied by the accumulation time in the experiment.

For Run 1, the discrepancy is mostly due to the dispersion of the concentration distribution during the detection phase of the experiment. There are three dispersion sources—the finite length heater, mixing in the tube connections between the test column and the TCD, and mixing in the detector cell. The dispersion resulting from the long heater is estimated by space-averaging the accumulation distribution over an effective heater width, which is the length along the tube between the sublimation start point and the dry-out point as the heater moves along the tube. The effective width is less than 2 cm while the accumulation is distributed over a length of 30 cm. The calculated dispersion due to heating length is very small when compared with the overall dispersion. The dispersion at the detector cell is estimated by a first-order (in time) model with a time constant. Since the time constant is about the response time of the cell (1 s), the concentration wave is little dispersed at the detector cell except some tailing effect of the wave, which results in the dispersion near $x = 0$.

Most of the dispersion occurs in between the test column and the detector. Especially, the dead volumes in the tube fittings and the control valves are responsible for most of the dispersion. The mechanism of the dispersion is basically convection-augmented molecular diffusion [12], which has been widely studied because of its importance in gas chromatography. An analytical estimate for the dispersion in the specific apparatus is not easy, nor is it crucial for the interpretation of the results. However, it should be mentioned that there exists an optimum flow velocity for the minimum dispersion [13, 14]. For a smaller flow rate than the optimum, more time is allowed for the axial molecular diffusion and for a larger flow rate, the contaminant is more dispersed by the radial variation of axial velocity.

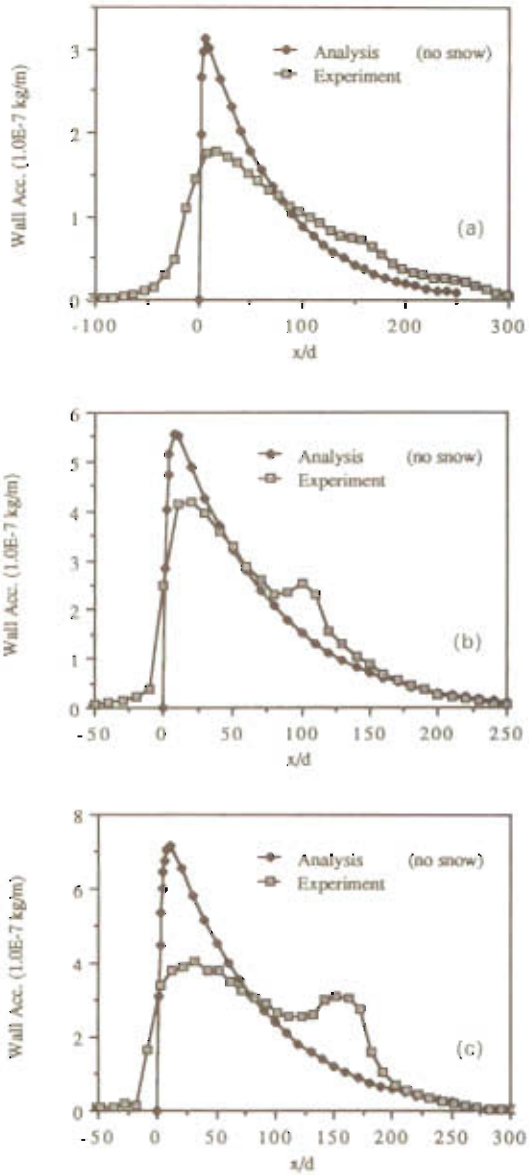

FIG. 7. Experimental and analytical distributions of wall accumulation: (a) Run 1; (b) Run 2; (c) Run 3.

For Run 2, the flow rate is near the optimum, thus the dispersion is small. The experimental distribution is in very good agreement with the analytical one except for a small secondary peak at $x/d \approx 100$. The

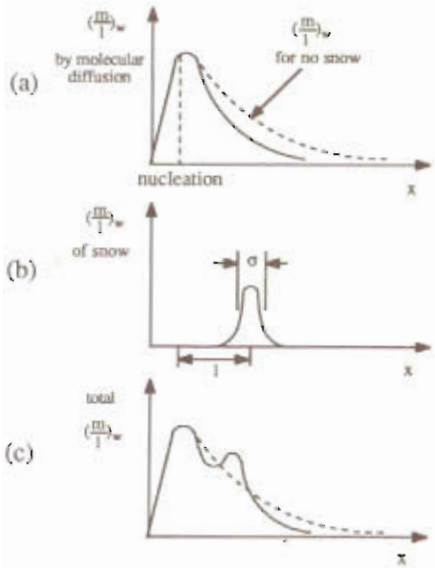

FIG. 8. Effect of snow formation on distribution of wall accumulation: (a) accumulation by molecular diffusion; (b) deposition of snow formed in free stream; (c) overall distribution of wall accumulation.

secondary peak is due to the snow formed by homogeneous nucleation in the supersaturated regions. The formation of snow moves some of the deposition downstream as explained in the next paragraph.

The degree of supersaturation increases with x until the concentration profile is fully developed and then decreases as discussed in ref. [9]. Thus any homogeneous nucleation of the supersaturated contaminant will occur in the mass transfer entrance region, which is $0 \leq x \leq 8$ for Run 2. As sketched in Fig. 8(a), as the nucleation starts in the entrance region, the accumulation by the molecular diffusion of contaminant to the tube wall is decreased because the radial gradient of concentration at the wall is smaller. On the other hand, the snow formed in the free stream is convected downstream with the gas and then deposited on the wall as shown in Fig. 8(b). The deposition displacement length, l, and deposition width, σ, are expected to be determined by the size and shape of snow crystals, the radial position of nucleation, the gas velocity, the surface condition of frost on the wall, and so on. The total mass accumulated on the wall has the shape shown in Fig. 8(c), which is similar to the experimental distribution of Run 2. With this reasoning, it is estimated that at least 2% of the total contaminant condensed as snow and was carried about 100 times the tube diameter before it was deposited on the wall over a width of 40 times the diameter.

For Run 3, the dispersion is larger than for Run 2 because the flow velocity exceeds the optimum. The amount of formed snow is at least 11% of total contaminant, which is greater than for Run 2 because the degree of supersaturation is greater. It is clear that the supersaturation increases as the flow velocity or the axial temperature gradient increase. The snow deposition displacement length and the deposition width are about 150 times and 60 times the tube diameter, respectively, for Run 3.

The dimensionless degree of supersaturation is a useful parameter for predicting the onset of snow formation of contaminants in helium for various flow conditions. The parameter depends on the concentration and temperature distributions for the no-snow case. The definition for the degree of supersaturation from ref. [9] is

$$\mathrm{DSS} = \frac{c_p \Delta T_{max}}{h_{ig}} \tag{7}$$

where ΔT_{max} is the maximum value of the difference between the local temperature and the saturation temperature corresponding to the local partial pressure of contaminant, c_p the specific heat of the vapor phase and h_{ig} the latent heat of sublimation of contaminant. The DSS indicates how much on an energy basis the contaminant has gone over the saturation point without a phase change, compared with the latent heat. The estimated values of DSS for Runs 1, 2, and 3 are 5.1×10^{-5}, 8.9×10^{-5}, and 1.1×10^{-4}, respectively. For various other flow conditions, the transition from no-snow to snow formation was observed within a narrow range of DSS centered on 8×10^{-5} (for details, see ref. [11]).

Finally, it should be mentioned that an application of the experimental apparatus to wider ranges of condition was restricted by excessive dispersion of the accumulation distribution.

4. SUMMARY AND CONCLUSIONS

A new experimental technique was developed to measure the mass transfer of a supersaturated contaminant to the wall of a heat exchanger tube with an axially linear temperature gradient. After the contaminant had accumulated on the wall as frost, the spatial distribution was converted to concentration vs time by propagating a steep temperature wave along the tube. The concentration history was measured by a detector at the tube exit. The measured distributions were compared with an analytical solution without homogeneous nucleation of snow. When the degree of supersaturation exceeded a specific value, the measured accumulation changed indicating the formation of snow that was carried downstream and then deposited on the wall.

REFERENCES

1. R. Barron, *Cryogenic Systems*, pp. 271–274. McGraw-Hill, New York (1966).
2. B. M. Bailey, Freeze out purification gases in heat exchangers. In *Advances in Cryogenic Engineering*, Vol. 2, pp. 45–49. Plenum, New York (1956).
3. O. E. Schupp III, *Gas Chromatography*, pp. 162–165. Interscience, New York (1968).

4. M. M. Chen, Heat transfer in heat exchangers under frosting conditions, Ph.D. Thesis, Department of Mechanical Engineering, Massachusetts Institute of Technology, Cambridge, Massachusetts (1960).
5. M. M. Chen and W. Rohsenow, Heat, mass, and momentum transfer inside frost tubes—experiment and theory, *ASME J. Heat Transfer* 334–340 (1964).
6. G. J. Trammell, D. C. Little and E. M. Killgore, A study of frost formed on a flat plate held at sub-freezing temperatures, *ASHRAE J.* **10**, 42–47 (1968).
7. J. L. Katz and B. J. Ostermier, Diffusion cloud-chamber investigation of homogeneous nucleation, *J. Chem. Phys.* **47**, 478–487 (1967).
8. R. R. Gilpin, Ice formation in a pipe containing flows in the transition and turbulent regions, *Int. J. Heat Mass Transfer* **103**, 363–368 (1981).
9. H.-M. Chang and J. L. Smith, Mass transfer analysis of contaminants in cryogenic helium systems : prediction of wall accumulation and snow formation, 7th Intersociety Cryogenic Symposium, Houston, Texas, 22–25 January (1989).
10. J. Sellars, M. Tribus and J. Klein, Heat transfer to laminar flow in a round tube or flat conduit—the Graetz extended problems, *Trans. ASME* **78**, 441–448 (1956).
11. H.-M. Chang, On the behavior of contaminants in cryogenic helium refrigeration systems, Ph.D. Thesis, Department of Mechanical Engineering, Massachusetts Institute of Technology, Cambridge, Massachusetts (1988).
12. G. I. Taylor, Dispersion of soluble matter in solvent flowing slowly through a tube, *Proc. R. Soc. London* **A219**, 186–203 (1953).
13. J. C. Giddings, *Dynamics of Chromatography, Part 1, Principles and Theory*, pp. 279–286. Marcel Dekker, New York (1965).
14. V. R. Maynard and E. Grushka, Measurement of diffusion coefficient by gas chromatography broadening techniques : a review. In *Advances in Gas Chromatography*, Vol. 12, pp. 99–140. Marcel Dekker, New York (1975).

TRANSFERT DE MASSE DE CONTAMINANTS SURSATURES DANS DES ECHANGEURS THERMIQUES CRYOGENIQUES A HELIUM

Résumé—Une nouvelle technique expérimentale est développée pour mesurer la distribution de givre accumulé dans le passage d'un échangeur thermique cryogénique à helium. Le givre est accumulé par condensation d'un contaminant sur la paroi pendant l'opération d'écoulement permanent de l'échangeur à contre-courant. La distribution est mesurée en faisant passer le contaminant accumulé dans un détecteur à la sortie du passage. Une source thermique est déplacée de l'extrémité froide vers la chaude pour convertir la distribution spatiale de contaminant en concentration ceci en fonction du temps dans le courant d'helium sortant. Quand le degré de sursaturation est faible, la distribution d'accumulation s'accorde raisonnablement bien avec la solution analytique sans formation de neige. Quand la sursaturation augmente, un pic secondaire net est observé dans la distribution à cause de la formation de neige dans l'écoulement libre et de son dépôt sur la paroi. A partir de ces résultats, une condition est formulée pour la formation en neige d'un contaminant sursaturé dans l'helium.

STOFFTRANSPORT VON ÜBERSÄTTIGTEN VERUNREINIGUNGEN IN KRYOTECHNISCHEN HELIUMWÄRMETAUSCHERN

Zusammenfassung—Ein neues experimentelles Verfahren zur Messung der Verteilung von Reif im Durchlaß eines Heliumwärmetauschers wird vorgestellt. Der Reif sammelt sich durch Kondensation von Verunreinigungen an der Wand des Durchlasses beim stationären Betrieb eines Gegenstromwärmetauschers. Die Verunreinigungen werden zum Ende des Durchlasses gespült und dort von einem Detektor nachgewiesen. Eine Wärmequelle wird vom kalten zum warmen Ende bewegt, um die räumliche Verteilung der Verunreinigung in eine zeitliche Konzentrationsverteilung im austretenden Heliumstrom zu übertragen. Wenn der Grad der Übersättigung klein ist, stimmt die Verteilung der Ausfällung gut mit der analytischen Lösung ohne Bildung von Schnee überein. Bei steigender Übersättigung wird ein deutlicher Sekundär-Peak in der Verteilung beobachtet, der von der Ausfällung von im freien Strahl entstandenem Schnee herrührt. Hieraus wird eine Bedingung für den Beginn der Schneebildung aus übersättigten Verunreinigungen in Helium entwickelt.

МАССОПЕРЕНОС ПЕРЕСЫЩЕННЫХ ПРИМЕСЕЙ В НИЗКОТЕМПЕРАТУРНЫХ ГЕЛИЕВЫХ ТЕПЛООБМЕННИКАХ

Аннотация—Разработан новый экспериментальный метод для измерения распределения инея в канале низкотемпературного гелиевого теплообменника. Иней образуется за счет конденсации примеси на стенке канала при работе равновесного противоточного теплообменника в стационарном режиме. Распределение инея измеряется путем заполнения детектора, установленного на выходе из канала, аккумулированной примесью. Для преобразования пространственного распределения примеси в концентрацию как функцию времени в вытекающем потоке гелия источник тепла перемещается от холодного торца к нагретому. При малой степени пересыщения распределение инея хорошо согласуется с аналитическим решением для случая без снегообразования. С ростом пересыщения отчетливо наблюдается вторичный пик в распределении, вызванный образованием снега при свободном течении и его последующим оседанием на стенке в виде инея. На основе полученных результатов найдено условие начала снегообразования пересыщенной примеси в гелии.